Journal of
Ceramic Science
and Technology

J. Ceram. Sci. Tech., 07 [01] 113-118 (2016)
DOI: 10.4416/JCST2015-00037
available online at: http://www.ceramic-science.com

Effects of *In-Situ*-Formed $9Al_2O_3{\cdot}2B_2O_3$ on the Corrosion Resistance of Al_2O_3-Based Porous Ceramic in Molten Aluminum

R. Xiang, Y. Li*, D. Xiang, N. Li, S. Li, Y. Li, S. Sang

The State Key Laboratory of Refractories and Metallurgy, Wuhan University of Science and Technology, Wuhan 430081, PR China

received July 23, 2015; received in revised form October 23, 2015; accepted November 11, 2015

Abstract

White fused alumina (WFA), α-Al_2O_3 powder, aluminum hydroxide powder and pseudoboehmite powder (PB) are each mixed with boric acid according to the stoichiometric ratio of $9Al_2O_3{\cdot}2B_2O_3$ in order to study the formation process. For the corrosion experiment, Al_2O_3-based porous ceramic with and without the addition of boric acid is prepared and soaked in molten aluminum for 48 h at 870 °C. The results show that the synthesis temperature of $9Al_2O_3{\cdot}2B_2O_3$ is 1000 °C, except for the mixture of PB and boric acid for which the synthesis temperature is 900 °C. The corrosion resistance of the samples with the addition of boric acid in molten aluminum is improved because of the generation of $9Al_2O_3{\cdot}2B_2O_3$ around the pores.

Keywords: Porous ceramic, in-situ synthesization, $9Al_2O_3{\cdot}2B_2O_3$, molten aluminum, corrosion resistance

I. Introduction

In the aluminum industry, static degassing is generally used to refine molten aluminum because of its many advantages such as simple components, high efficiency and low maintenance [1]. As effective degassing is related to bubble distribution and fine bubble size, the porous ceramic – called the porous plug, which is installed at the bottom of the refractory aluminum-containing vessel and enables the efficient flow of gas into the aluminum melt, is important for the aluminum refining. However, to the best of our knowledge, only few reports are available on the corrosion resistance of the porous plug.

It has been suggested that, in the manufacture of the refractory plug, the addition of specific additives, namely non-wetting agents, can lower the wettability of the refractory when exposed to molten aluminum and thereby reduce aluminum penetration into the refractory [2], thus enhancing its corrosion resistance. Many compounds like $BaSO_4$, CaF_2, AlF_3 and certain rare-earth oxides are considered useful agents [3–5] Especially the low solubility of boron in molten aluminum alloys is an advantage of the use of these additives in refractories for melting Al alloys [5–6].

$9Al_2O_3{\cdot}2B_2O_3$ is a binary compound in the phase diagram of the Al_2O-B_2O_3 system with mullite-like properties such as outstanding mechanical properties, excellent resistance to corrosion, and chemical stability [7–8]. It is widely used as whiskers in oxidation-resistant and whisker-reinforced composites because of its low-cost production and easy fabrication in large quantities [7–9]. In this study, boric acid is mixed with different materials according to the stoichiometric ratio of $9Al_2O_3{\cdot}2B_2O_3$ to study the formation process, and Al_2O_3-based porous ceramics with boric acid are prepared to evaluate their corrosion resistance when exposed to molten aluminum.

* Corresponding author: lybref2002@126.com

II. Experimental Procedure

White fused alumina (WFA), α-Al_2O_3 powder, aluminum hydroxide powder, pseudoboehmite powder (PB) and boric acid powder (AR, Sinopharm Chemical Reagent Co. Ltd., China) are used as raw materials. The chemical compositions determined by means of induced coupled plasma emission spectroscopy (ICP) are shown in Table 1, furthermore, the median particle diameters of the WFA powder, α-Al_2O_3 powder, aluminum hydroxide and PB are 30.57 μm, 2.34 μm, 43.75 μm and 3.69 μm respectively.

The mass ratios of WFA powder/boric acid powder (CH), α-Al_2O_3 powder/boric acid powder (AH), aluminum hydroxide powder/boric acid powder (AOH) and PB/boric acid powder (PBH) correspond to the stoichiometric ratio of $9Al_2O_3{\cdot}2B_2O_3$. After homogeneous mixing of the powders in the dry state, cylindrical green compacts measuring 20 mm in diameter and 20 mm in thickness were prepared by means of die-pressing at 200 MPa for each mixed powder. The compacts were fired at a temperature varied from 800 °C to 1600 °C for 3 h with a heating rate of 2 K/min.

The particle size was measured with a laser particle size analyzer (Mastersizer2000, Malvern Instruments Ltd., UK). Phase compositions and the microstructure of the samples were characterized by means of X-ray diffraction with Cu-Kα radiation (XRD, X'Pert Pro, Philips, Netherlands) and scanning electron microscopy (SEM, XL-30TMP, Philips, Netherlands). An electron probe microanalyzer (EMPA, JXA8800, JEOL, Japan) was used to analyze the distribution of the boron. Bulk density was

Table 1: Chemical composition of raw materials (wt%)

Raw material	Al_2O_3	SiO_2	Fe_2O_3	CaO	MgO	K_2O	Na_2O	H_3BO_3	I.L.
WFA	98.61	0.24	0.43	-	-	0.29	0.08	-	0.22
α-Al_2O_3 powder	98.54	0.18	0.12	-	-	0.35	0.07	-	0.33
Mild-clay	31.85	50.69	2.18	0.79	0.29-	1.07	0.13	-	10.61
Aluminum hydroxide	64.86	0.08	0.06	0.04	0.02	0.04	0.01	-	34.44
PB	80.52	0.26	0.05	0.50	0.13	0.02	0.29	-	18.06

measured according to the Archimedes method using distilled water as liquid media, and the pore size distribution was characterized by means of mercury porosimetry (AutoPore IV9510, Micromeritics, USA).

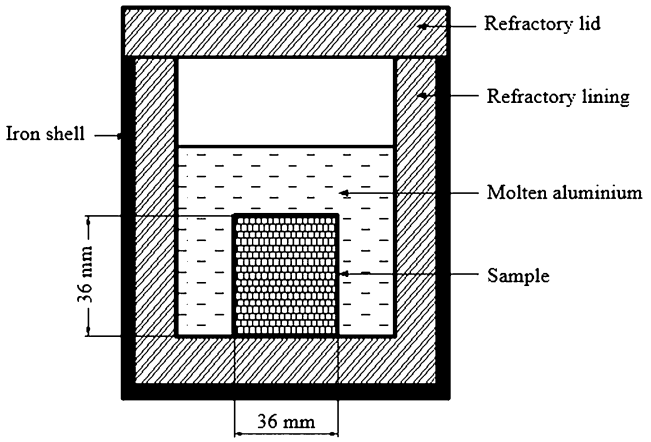

Fig. 1: Diagrammatic sketch of a sample soaking in molten aluminum.

As the green samples are expected to shrink or swell when exposed to heat treatment, diameters were measured before and after sintering to characterize the linear change rate dimensionally using the following equation:

$$S(\%) = \frac{d_a}{d_b} - 1 \quad (1)$$

where d_b refers to an average value for a green sample based on three diameters measured at the top, middle and bottom, d_a is obtained in the same way for the same sample after sintering.

The corrosion resistance testing equipment is shown in Fig. 1, samples are soaked in the molten alumina for 48 h at 870 °C and cut along the axis after they have cooled.

III. Results and Discussion

XRD patterns of each compact sintered at different temperatures are shown in Fig. 2. Boric acid decomposes into B_2O_3 at about 250 °C and melts at about 450 °C [10]. In Fig. 2A, WFA reacts with boric acid at 900 °C to form $2Al_2O_3{\cdot}B_2O_3$. At 1000 °C, $9Al_2O_3{\cdot}2B_2O_3$ is synthesized at the expense of $2Al_2O_3{\cdot}B_2O_3$, the intensity of $9Al_2O_3{\cdot}2B_2O_3$ increases up to 1300 °C, but decreases at higher temperatures, and the phase evolutions of AH in Fig. 2B is similar to that of CH.

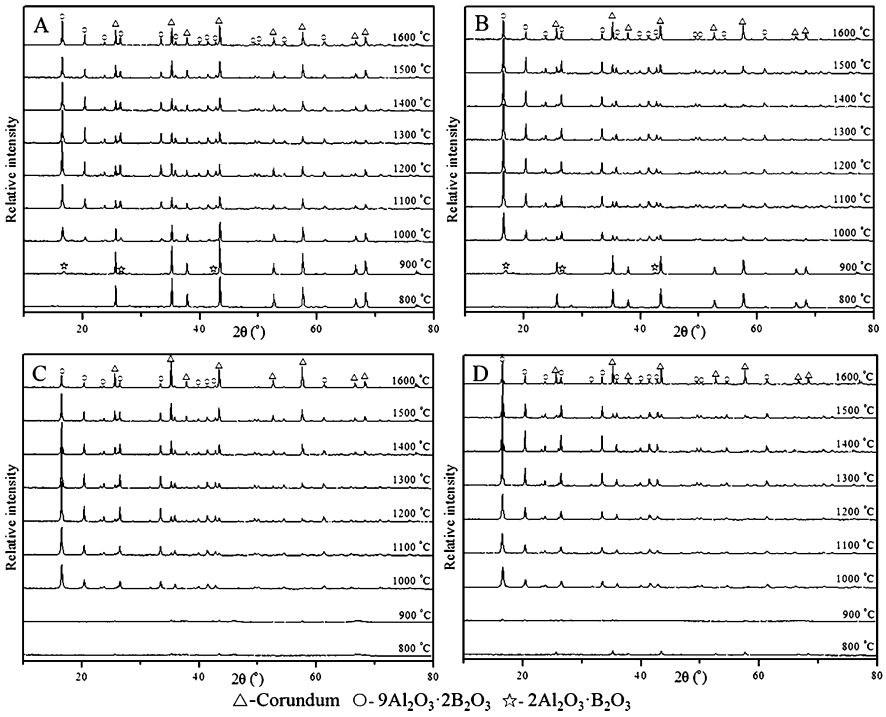

Fig. 2: Phase evolutions for A sample CH, B sample AH, C sample AOH and D sample PBH with temperature.

Fig. 2C shows the XRD patterns of AOH, a small amount of corundum is detected in the samples sintered at 800 °C and 900 °C as the decomposition products of aluminum hydroxide. The peak intensity of $9Al_2O_3 \cdot 2B_2O_3$ becomes obvious at 1000 °C and reaches its maximum at 1300 °C. On account of the B_2O_3 volatilization prone to occur at higher temperatures, less $9Al_2O_3 \cdot 2B_2O_3$ is detected at 1400 °C and higher temperatures. As can be seen in Fig. 2D, corundum appears at 800 °C and reacts with boric acid to form $9Al_2O_3 \cdot 2B_2O_3$ at 900 °C, the lower temperature of the formation of $9Al_2O_3 \cdot 2B_2O_3$ compared with that of AOH can be attributed to the smaller particle size. Furthermore, according to the phase diagram of Al_2O_3-B_2O_3 [11], $9Al_2O_3 \cdot 2B_2O_3$ decomposes into corundum and liquid phase at 1430 °C and this can explain the corundum at 1500 °C.

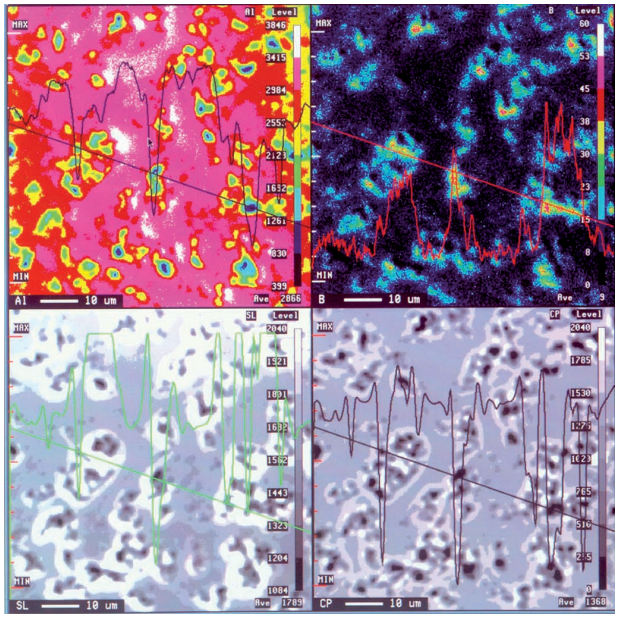

Fig. 3: EPMA patterns of PBH mixture powder heated at 1400 °C.

Fig. 3 shows the distribution of boron in the PBH sintered at 1400 °C. The content of boron at the pores is much higher than elsewhere. B_2O_3 volatilizes readily at high temperatures and concentrates at the pores during diffusion, Al_2O_3 around the pores reacts with the accumulated B_2O_3 to form $9Al_2O_3 \cdot 2B_2O_3$. The linear change rate of the various mixtures sintered from 800 to 1600 °C is plotted in Fig. 4. There is great similarity between the curves of CH and AH, both compacts shrink at 800 and 900 °C, and swell at 1000 °C. The shrinkage is observed again at 1400 °C and higher temperatures. Taking into consideration the phase evolution of corresponding compact, we come to the conclusion that expansion in the generation process of $9Al_2O_3 \cdot 2B_2O_3$at 1000 °C overcomes shrinkage in sintering and when the temperature is 1400 °C or higher, the volatilization of the B_2O_3 leads to shrinkage. However, in terms of the PBH and AOH, the contractive rate of PBH is obviously higher than that of the AOH owing to the much smaller particle size.

The microstructural variation of the AH at different temperatures is not evident as shown in Fig. 5, nor is the linear change. In Fig. 6, the number and size of the pores in AOH decrease with the increasing temperature, which leads to the increase in shrinkage. A significant number of pores are formed because the grains are refined as a result of volatilization of the B_2O_3 at higher temperatures. Compared with the AH and AOH, the microstructure of PBH in Fig. 7 is the densest and thus the maximum shrinkage has been achieved.

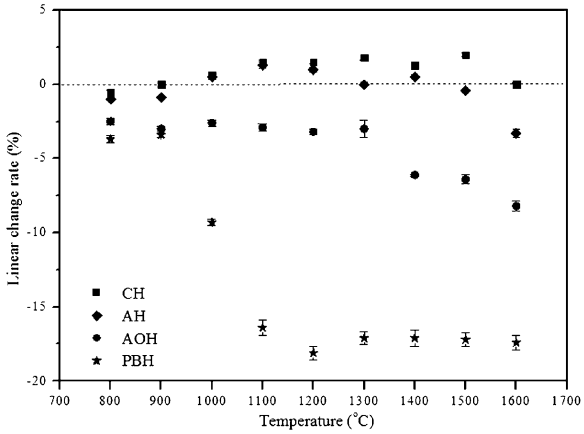

Fig. 4: Linear change rate of different samples at different temperatures.

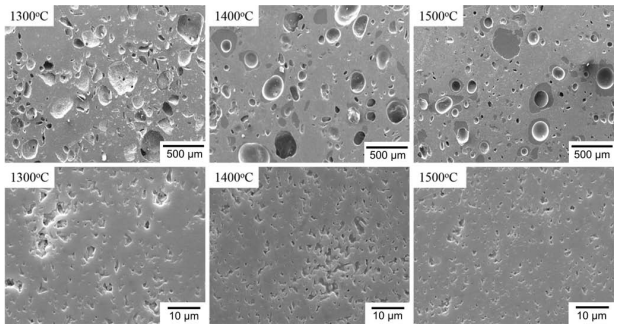

Fig. 5: SEM images of sample AH sintered at different temperatures.

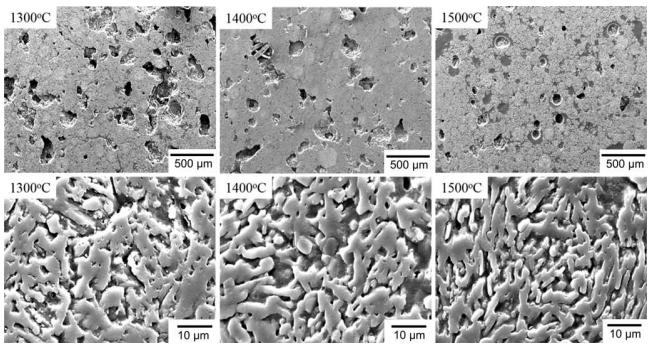

Fig. 6: SEM images of sample AOH sintered at different temperatures.

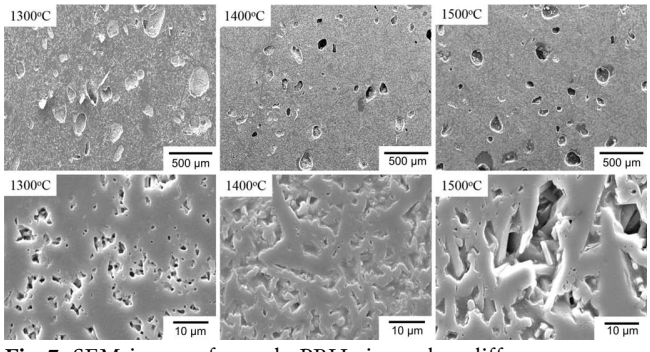

Fig. 7: SEM imagesof sample PBH sintered at different temperatures.

Table 2: Compositions of raw materials (wt%)

No.	WFA aggregate		WFA powder	α-Al_2O_3 powder	Aluminum hydroxide powder	PB
	Size distribution	Content				
1#	1 – 0.2 (mm)	70	15	10		
2#	1 – 0 (mm)	70	5	10	10	
3#	1 – 0.2 (mm)	60	10	15		10

Samples for the corrosion resistance test are prepared according to Table 1 and Table 2 respectively. The mass ratio of aggregate/powder for Sample 1, 2, and 3 in Table 2 is consistent with that of 1#, 2# and 3# in Table 1 respectively, and the binding agent for all the samples is 5 wt% silicon-sol. The mixture of AOH and PBH is added to the samples with the precondition of keeping the mass fraction of aluminum hydroxide and PB in Table 2 the same as those in Table 1. CH and AH are also added in order to maintain the mass ratio of WFS powder/α-Al_2O_3. The profiles of the samples after testing are shown in Fig. 8, Fig. 9 and Fig. 10. For the Sample 1 sintered at 1200 °C and 1300 °C, no traces of permeation is found, profiles of the samples sintered at 1400 °C are darker than those at the other temperatures, probably caused by the permeation of the aluminum steam. Profiles of Sample 2 with boric acid addition become darker but the ones without the addition of boric acid are mostly permeated. Besides, there is almost no permeation in the Sample 3. It is evident that, after the addition of boric acid, the generation of $9Al_2O_3 \cdot 2B_2O_3$ can effectively prevent the samples from being penetrated by the molten aluminum.

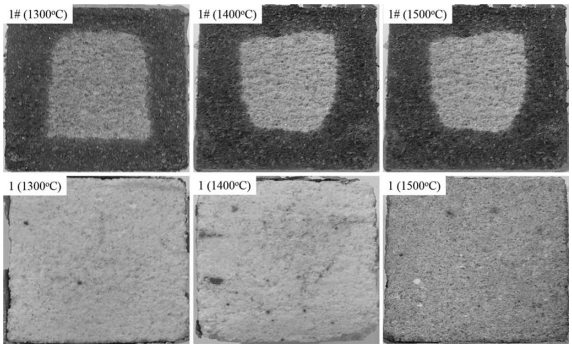

Fig. 8: Camera photographs of the profiles of Sample 1# and Sample 1 sintered at different temperatures after the corrosion resistance test.

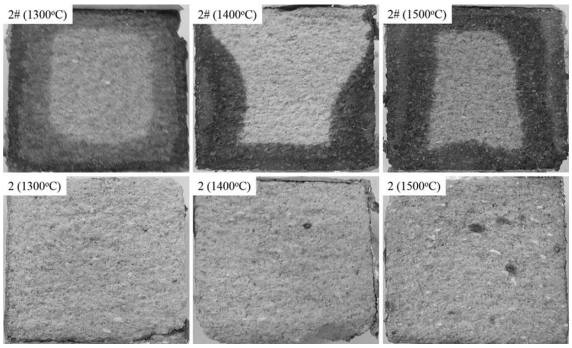

Fig. 9: Camera photographs of the profiles of Sample 2# and Sample 2 sintered at different temperatures after the corrosion resistance test.

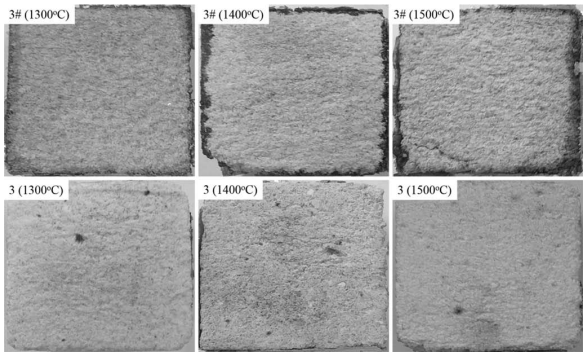

Fig. 10: Camera photographs of the profiles of Sample 3# and Sample 3 sintered at different temperatures after the corrosion resistance test.

The pore size distributions of Samples 2# and 2 are measured by means of mercury intrusion and shown in Fig. 11, the addition of boric acid increases the number of pores with larger size, therefore the improved corrosion resistance is due to the generation of $9l_2O_3 \cdot 2B_2O_3$. Adabifiroozjaei *et al.* studied the effect of different boron-containing materials (B_2O_3, B_4C, and BN) on the corrosion resistance of aluminosilicate refractories [6]. The improvement in corrosion resistance is attributed to the high stability of $9Al_2O_3 \cdot 2B_2O_3$ phase as well as the low solubility of boron in molten aluminium alloys. Moreover, the better resistance can also be related to the decrease in the degree of wetting of molten aluminum on the solid ceramics [4]. Further investigation is required to evaluate the change in the wetting angle effected by the addition of boric acid.

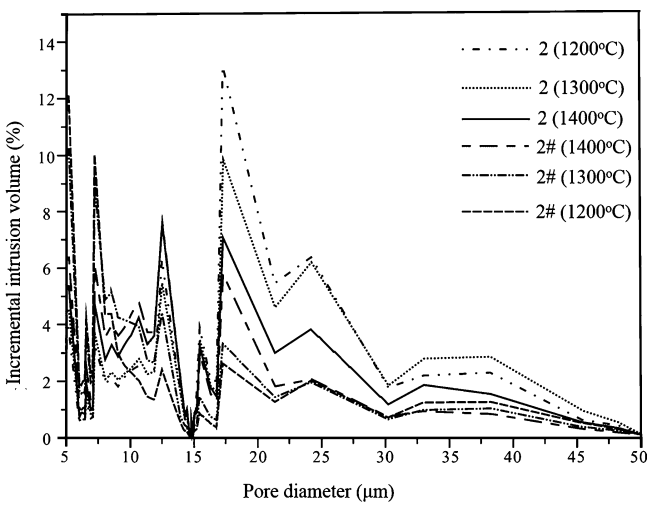

Fig. 11: Pore size distribution of Samples 2 and 2# with and without boric acid, sintered at different temperatures.

Table 3: Compositions of raw materials (wt%)

No.	WFA aggregate		WFA powder	α-Al_2O_3 powder	Aluminum hydroxide powder	PB	Boric acid
	Size distribution	Content					
1	1 – 0.2 (mm)	70	11.81	7.87			5.22
2	1 – 0 (mm)	70	3.46	6.93	10		4.43
3	1 – 0.2 (mm)	60	7.16	10.7		10	7.14

IV. Conclusions

The synthesis temperature of $9Al_2O_3{\cdot}2B_2O_3$ is 1000 °C for the CH, AH and AOH samples, and 900 °C for PBH samples. The microstructure of the AH samples is not sensitive to temperature variation from 1300 °C to 1500 °C, but the increasing temperature leads to the formation of a significant number of pores in the AOH and PBH samples. $9Al_2O_3{\cdot}2B_2O_3$ is mostly distributed around the pores in the samples because of the concentrate of B_2O_3 resulting from the B_2O_3 volatilization. The corrosion resistance on exposure to molten aluminum is improved with the addition of boric acid, which is due to the generation of $9Al_2O_3{\cdot}2B_2O_3$.

References

1 Larsen, D.A.: Degassing aluminum using static fine-pore refractory diffusers, *JOM*., **49**, [8], 27 – 28, (1997).

2 Afshar, S., Allaire, C.: Furnaces: improving low cement castables by non-wetting additives, *JOM*., **53**, [8], 24 – 27, (2001).

3 Obrien, M.H., Akinc, M.: Reduction in aluminum alloy attack on aluminosilicate refractories by addition of rare-earth oxides, *J. Am. Ceram. Soc.*, **73**, 491 – 495, (1990).

4 Aguilar-Santillan, J.: Wetting of Al_2O_3 by molten Aluminum: the influence of $BaSO_4$ additions, *J. Nanomater.*, **4**, 145 – 152, (2008).

5 Adabifiroozjaei, E., Koshy, P., Sorrell, C.C.: Assessment of non-wetting materials for use in refractories for aluminium melting furnaces, *J. Aust. Ceram. Soc.*, **51**, 139 – 145, (2015).

6 Adabifiroozjaei, E., Koshy, P., Sorrell, C.C.: Effects of different boron compounds on the corrosion resistance of andalusite-based low-cement castables in contact with molten al alloy, *Metall. Mater. Trans. B*, **43**, 5 – 13, (2012).

7 Wang, J., Ning, G., Lin, Y.: Chemical synthesis of $Al_{18}B_4O_{33}$ whiskers via a combustion method, *Mater. Lett.*, **62**, 2447 – 2449, (2008).

8 Douy, A., Aluminium borates: synthesis via a precipitation process and study of their formation by DSC analysis, *Solid State Sci.*, **7**, 117 – 122, (2005).

9 Fischa, M., Armbruster, T., Rentsch, D., Libowitzky, E., Pettke, T.: Crystal-chemistry of mullite-type aluminoborates $Al_{18}B_4O_{33}$ and Al_5BO_9: A stoichiometry puzzle, *J. Solid State Chem.*, **184**, 70 – 80, (2011).

10 Wang, J., Sha, J., Yang, Q., Wang, Y.W., Yang, D.R.: Synthesis of aluminium borate nanowires by sol-gel method, *Mater. Res. Bull.*, **40**, 1551 – 1557, (2005).

11 Levin, E.M., Robbins, C.R., McMurdie, H.F.: Phase diagrams for ceramicists, The American Ceramic Society, Inc., USA, 1987.